




Article

Dust-Acoustic Nonlinear Waves in a Nanoparticle Fraction of Ultracold (2K) Multicomponent Dusty Plasma

Fedor M. Trukhachev ^{1,2,3,*} , Roman E. Boltnev ^{1,3,4} , Mikhail M. Vasiliev ^{1,3}  and Oleg F. Petrov ^{1,3}

¹ Joint Institute for High Temperatures of the Russian Academy of Sciences, 125412 Moscow, Russia; boltnev@gmail.com (R.E.B.); mixxy@mail.ru (M.M.V.); ofpetrov@ihed.ras.ru (O.F.P.)

² Belarusian-Russian University, 212000 Mogilev, Belarus

³ Moscow Institute of Physics and Technology, 141701 Dolgoprudny, Russia

⁴ Chernogolovka Branch of the N.N. Semenov Federal Research Center for Chemical Physics, Russian Academy of Sciences, 142432 Chernogolovka, Russia

* Correspondence: ftru@mail.ru

Abstract: The nonlinear dust-acoustic instability in the condensed submicron fraction of dust particles in the low-pressure glow discharge at ultra-low temperatures is experimentally and theoretically investigated. The main discharge parameters are estimated on the basis of the dust-acoustic wave analysis. In particular, the temperature and density of ions, as well as the Debye radius, are determined. It is shown that the ion temperature exceeds the temperature of the neutral gas. The drift characteristics of all plasma fractions are estimated. The reasons for the instability excitation are considered.

Keywords: ultracold dusty plasma; nonlinear dusty-acoustic wave; Debye radius



Citation: Trukhachev, F.M.; Boltnev, R.E.; Vasiliev, M.M.; Petrov, O.F. Dust-Acoustic Nonlinear Waves in a Nanoparticle Fraction of Ultracold (2K) Multicomponent Dusty Plasma. *Molecules* **2022**, *27*, 227. <https://doi.org/10.3390/molecules27010227>

Academic Editor: Marek Kosmowski

Received: 17 November 2021

Accepted: 27 December 2021

Published: 30 December 2021

Publisher's Note: MDPI stays neutral with regard to jurisdictional claims in published maps and institutional affiliations.



Copyright: © 2021 by the authors. Licensee MDPI, Basel, Switzerland. This article is an open access article distributed under the terms and conditions of the Creative Commons Attribution (CC BY) license (<https://creativecommons.org/licenses/by/4.0/>).

1. Introduction

Dusty plasma is a plasma containing fractions of charged microparticles along with electrons and ions. Such plasmas are common in space and have many technological applications [1]. The main methods of dust fraction formation are injection of dust particles in plasma, chemical reactions in plasma, and ion sputtering of various materials in plasma [1]. In rare and poorly studied cases, several mechanisms are involved simultaneously [2]. The presence of low-frequency wave modes is one of the features of dusty plasma. For example, the frequencies of well-understood dust-acoustic waves are in the range of 0.1–100 Hz.

In recent years, studies of cryogenic dusty plasma have become relevant, which is due to various fundamental and technological aspects [3–10]. Notably, the study of ultra-low-temperature discharges is an independent physical problem [11–13]. Among the open questions, one can single out the gas-to-ion temperature ratio, the magnitude of the screening scale, etc. For example, dusty plasma in a glow discharge at liquid nitrogen and helium temperatures was investigated in [4]. It was assumed that the temperatures of ions and neutral gas are equal. In this case, the ion Debye radius is of the order of one micron at a gas temperature of 4.2 K, pressure $p = 4$ Pa, and the ratio of the electric field to the density of a neutral gas $E/N \sim 10$ Td. The same results are presented in a study by [6]. On the other hand, in [9], by studying the dust interparticle distance, it was found that the screening radius exceeds the Debye ionic radius by an order of magnitude assuming that the ionic and atomic temperatures are equal. Possible explanations for this phenomenon can be a nonlinear screening of a particle charge [14,15], overheating of ions in the discharge plasma [16–21], etc. Nevertheless, this issue remains open. The ion parameters were measured within a wide range of temperature and for different values of the E/N ratio using mass spectroscopy methods [16–18]. It was shown that in cryogenic discharges, at $E/N > 10$ Td, the effective temperature of the ions can exceed the temperature of the parent gas by an order of magnitude. These results are in good accordance with the conclusions

of recent theoretical [19,20] and experimental [21] works. A similar result, but for dusty plasma, was obtained in [22] both experimentally and in the framework of the Monte Carlo method. It also shows that the main ions in a cryogenic discharge are atomic helium He^+ ions if E/N exceeds 10 Td. Thus, the determination of the Debye radius and ion temperature in the cryogenic discharge remains an unsolved problem.

In this paper, the nonlinear dust-acoustic instability (with nonlinear waves excitation) in a multicomponent plasma at the buffer gas temperature of ~ 2 K (pressure $p = 5$ Pa, $E/N \sim 10$ Td) is studied in detail. The plasma consisted of electrons, helium ions, micron-sized particles injected into the discharge, and condensed nanoparticles. As mentioned above, the properties of such plasma configuration are poorly understood. We found only one publication [2], which describes the radio-frequency RF discharge plasma containing both injected and condensed (grown) dust fractions. Ion sputtering of the surface of the injected dust particles led to the formation of a condensed fraction. Recently, such multicomponent DC discharge plasma was investigated in [23–25]. In [23,24], wave processes were observed; however, they were not studied in detail. The proposed research is a logical continuation of works [23,24]. Dust-acoustic waves can be an effective tool for plasma diagnostics because their main parameters can be accurately measured. In turn, the wave parameters are related to the plasma parameters by known relations. In this research, wave analysis is carried out in the framework of a simple hydrodynamic model. The screening length, ion temperature, drift velocities, and some other discharge parameters are determined independently.

2. Results

2.1. Plasma Parameters

The wave process observed in the experiment (Section 4) is rather complex, and its detailed description is beyond the scope of this work. However, our estimates allow us to reasonably describe the observed phenomena.

The process begins with an estimate of the Debye radius— λ_D ; this problem at ultralow temperatures was discussed in [4,9,22]. For λ_D , we can write

$$\lambda_D^{-2} = \lambda_{De}^{-2} + \lambda_{Di}^{-2} \quad (1)$$

where $\lambda_{De,i} = (\epsilon_0 T_{e,i} / e^2 n_{e,i})^{1/2}$ are the Debye radii for electrons and ions, respectively. The width of the observed soliton-like dust density profiles is $L \approx 100 \mu\text{m}$ (See Section 4). As follows from theoretical work [26], large-amplitude dust-acoustic soliton widths are about $1\text{--}3 \lambda_D$. The width of the soliton was meant the width of the dust density profile. This parameter is easy to measure experimentally; thus, it is analogous to “standard candles” in astrophysics. In our case, $\Delta_+ \approx 100 \mu\text{m}$, therefore, we have $\lambda_D \approx 30\text{--}100 \mu\text{m}$, which agrees well with [9,22] and significantly exceeds the estimates presented in [4,6]. We set $\lambda_D = 30 \mu\text{m}$; that is, we assume that the width of the wave crest density profile contains at least three Debye radii (upper bound from the study by [26]). From Equation (1) and data in Table 1, it follows that λ_D corresponds to the ion Debye radius $\lambda_D = \lambda_{Di}$, which indicates that the ion drift is subsonic. With supersonic drift, we have $\lambda_D = \lambda_{De}$ (see, for example, [27]). In this case, by setting $T_e \approx 1$ eV (Table 2), we have $\lambda_{De} \gg \lambda_{Di}$; therefore, the width of the nonlinear wave profiles should be much larger than the observed value.

Table 1. The main parameters of the plasma.

Plasma Parameters	Value
Neutralgas pressure.	$P_{\text{He}} = 5 \text{ Pa}$
Discharge current	$I = 35 \pm 15 \text{ }\mu\text{A}$
Discharge voltage	$U = 3.21 \text{ kV}$
Neutralgas density	$n_{\text{He}} = 1.8 \times 10^{23} \text{ m}^{-3}$
Temperature of the neutral gas (the walls of the discharge tube)	$T_a \approx 2 \text{ K}$
Radius of the first fraction dust particles	$r_{d1} \approx 1\text{--}5 \text{ }\mu\text{m}$
Radius of the second fraction dust particles	$r_{d2} \approx 15\text{--}35 \text{ nm}$
Mass density of the first fraction dust particles	$\rho_1 = 7200 \text{ kg/m}^3$
Mass density of the second fraction dust particles	$\rho_2 = 1100\text{--}1500 \text{ kg/m}^3$
Electric field strength	$E \approx 2000 \text{ V/m}$
Reduced electric field strength	$E/N \approx 10 \text{ Td}$

Table 2. Calculated plasma parameters.

Plasma Parameters	Value
Density of the first fraction particles	$n_{d1} = 3.0 \times 10^5 \text{ cm}^{-3}$
Density of the second fraction particles	$n_{d2} = 3.7 \times 10^7 \text{ cm}^{-3}$
Charge of the first fraction dust	$Z_1 \approx 500$
Charge of the second fraction dust	$Z_2 = 2$
Electron density	$n_e \approx 1 \times 10^7 \text{ cm}^{-3}$
Ion density	$n_i \approx 2.3 \times 10^8 \text{ cm}^{-3}$
Electron temperature	$T_e \approx 10^4 \text{ K}$
Ion temperature	$T_i \approx 45 \text{ K}$
Electron Debye length	$\lambda_{De} = 2.2 \times 10^{-1} \text{ cm}$
Ion Debye length	$\lambda_{Di} = 3.0 \times 10^{-3} \text{ cm}$
Ion free path	$l_i = 5.5 \text{ }\mu\text{m}$
Gravitational force for the first fraction particles	$F_{G1} = 1.6 \times 10^{-13} \text{ N}$
Gravitational force for the second fraction particles	$F_{G2} = 2.0 \times 10^{-18} \text{ N}$
Electric force for the first fraction particles	$F_{E1} = 1.6 \times 10^{-13} \text{ N}$
Electric force for the second fraction particles	$F_{E2} = 3.2 \times 10^{-16} \text{ N}$
Ion drag force for the first fraction particles	$F_{id1} = 3.0 \times 10^{-14} \text{ N}$
Ion drag force for the second fraction particles	$F_{id2} = 4.9 \times 10^{-18} \text{ N}$
Neutral drag force for the first fraction particles at $u_{0d1} = 5 \times 10^{-3} \text{ m/s}$	$F_{nd1} = 1.6 \times 10^{-15} \text{ N}$
Neutral drag force for the second fraction particles at $u_{0d2} = 0.2 \text{ m/s}, \gamma = 1 + \pi/8$	$F_{nd2} = 2.2 \times 10^{-16} \text{ N}$
Electron thermal velocity	$v_{Te} = 4 \times 10^7 \text{ cm/s}$
Ion thermal velocity	$v_{Ti} = 3 \times 10^4 \text{ cm/s}$

Having λ_D one can estimate the initial density of dust particles of the second fraction— n_{0d2} . The density n_{0d2} is large enough for the effective scattering of laser radiation on the wave profile; however, in the unperturbed state, the condensed particles weakly scatter light. We assume that the particle charge is proportional to the radius as well as that $Z = 10^3$ for $r = 0.5 \text{ }\mu\text{m}$. Then, we obtain $Z_2 = 5$ for $r = r_{d2}$. According to [22,28,29] when the discharge temperature decreases to cryogenic values, Z decreases by 2–3 times, compared with normal conditions; thus, finally, we have $Z_2 = 1\text{--}2$. For such small

charges, it can be assumed that the interparticle distance is equal to the Debye radius $L_2 \approx \lambda_{Di} \approx 30 \mu\text{m}$, then $n_{0d2} = \lambda_{Di}^{-3} = 3.7 \times 10^7 \text{ cm}^{-3}$. Further, from the quasi-neutrality condition $n_{0i} - n_{0e} - Z_1 \cdot n_{0d1} - Z_2 \cdot n_{0d2} = 0$, we obtain $n_{0i} = n_{0e} + Z_1 \cdot n_{0d1} + Z_2 \cdot n_{0d2}$. Taking into account the data in Table 2, we can obtain $n_{0i} = 2.3 \times 10^8 \text{ cm}^{-3}$. Next, from (1), we obtain the estimate for the ion temperature $T_i = 45 \text{ K}$. Thus, analysis of the wave process implies $T_i \gg T_a$ at $E/N \approx 10 \text{ Td}$, which confirms the results of [16–20,22], obtained by other methods. The value of n_{0e} can be approximately estimated from the expression for the discharge current $I/S \approx j = en_{0e}u_{0e}$, where $S = \pi R^2$ is the cross-sectional area of the discharge tube, j is the current density, and u_{0e} is the drift velocity of electrons. For various glow discharge strata in different experiments $u_{0e}/v_{Te} \sim 0.1\text{--}1$, where $v_{Te} = (T_e/m_e)^{1/2}$ is an electron thermal velocity. Then, setting $I = 50 \mu\text{A}$ (the upper estimate for the discharge current in our experiment), we obtain $n_{0e} \sim I/\pi R^2 e A v_{Te} \sim 10^6\text{--}10^7 \text{ cm}^{-3}$, with $A = u_{0e}/v_{Te} = 0.1\text{--}1$. The value of n_{0e} on the discharge axis may be several times higher than the obtained estimate due to the radial inhomogeneity of the current. Finally, we estimate the mean free path of ions by the formula $l_i = (n_a \sigma_{in})^{-1}$ [30], where σ_{in} is the cross section for the scattering of ions on helium atoms. In accordance with the data listed in Table IIa from [18] $\sigma_{in} = 10^{-14} \text{ cm}^2$, with $T_a = 4.35 \text{ K}$ (there are no data at $T_a = 2 \text{ K}$) and $E/N = 10 \text{ Td}$, then $l_i = 5.5 \mu\text{m}$. Thus, $\lambda_D > l_i$ (the ions are collisional). The calculated data are provided in Table 2, according to which the forces acting on the dust particles need to be calculated.

2.2. The Main Forces

The ion drift velocity, in accordance with the data listed in Table IIa from [18], is $u_{0d2} = 5.2 \cdot 10^3 \text{ cm/s}$ at $E/N = 10 \text{ Td}$, considering that the main ions are He^+ [22]. It is worth noting that the type of ion is not so important for the estimates, since the mobilities of the He^+ , He_2^+ , and He_3^+ ions are not very different [31,32]. Assuming that $T_i = 45 \text{ K}$, we can obtain an estimate for the ion thermal velocity $v_{Ti} = (T_i/m_i)^{1/2} = 3.05 \times 10^4 \text{ cm/s}$, hence $u_{0d2} \ll v_{Ti}$.

In the vertical direction, the main forces to be considered are the gravitational force F_G , the electric force due to a vertical discharge electric field F_E , the neutral drag force F_{nd} , and ion drag force F_{id} . The first three forces are described by simple expressions as follows:

$$F_G = \frac{4}{3} \pi r_d^3 \rho_d g, \quad (2)$$

$$F_E = -e Z_a E, \quad (3)$$

$$F_{nd} = \frac{8}{3} \sqrt{2} \pi r_d^2 m_n n_n \gamma v_{Tn} v_{da} \equiv m_d v_{nd} v_{da} \quad (4)$$

where r_d and ρ_d are the radius and mass density of dust particles, $a = 1, 2$ for particles of the first and second fractions, respectively, $g = 981 \text{ cm/s}^2$, m_n , n_n , and $v_{Tn} = \sqrt{T_n/m_n}$ are the mass, density, and thermal velocity of the neutral gas atoms, respectively, v_{da} is the speed of dust particles relative to a neutral gas, v_{nd} is dust-neutral collision frequency, γ is a coefficient on the order of unity that depends on the exact processes proceeding on the particle surface, and γ takes values from 1 to $1 + \pi/8$ [1].

Ion drag forces were calculated in accordance with [33] (Equation (11)). The values of the main forces are provided in Table 2 (taking into account Table 1 data).

As can be seen from Table 2, for large particles (fraction «1»), gravity is balanced by electrostatic force. Large particles are visible, so their motion parameters can be easily determined. The large particles' speed is small, so the neutral drag force, as well as the ion drag force, can be neglected for them. Particles of fraction 2 are invisible, and only the modulation of their density caused by waves is available for observations. However, this is sufficient to determine the important parameters of particle motion. From Table 2, it follows that $F_E \approx F_{nd2} \gg F_G \sim F_{id2}$, i.e., the electric force can be balanced only by the neutral drag force in the presence of a drift $u_{0d2} \approx 20 \text{ cm/s}$, directed upwards. Taking into account the data of Tables 1 and 2 and putting $Z_2 = 2$, we obtain $u_{0d2}/C_{d2} = 4.7$, where $C_{d2} = \sqrt{\frac{Z_2^2 n_{0d2} T_e T_i}{m_{d2}(n_{0e} T_i + n_{0i} T_e)}}$ is the dust-acoustic speed for fraction 2 [34,35]. Thus, the drift of

fraction 2 is supersonic. Under these conditions, the phase state “liquid” or “gas” is most likely for fraction 2. The soliton-like wave crests move downward relative to the particles of the second fraction with a speed equal to or greater than u_{0d2} . At the same time, in a fixed coordinate system, the wave speed is $V_0 \leq 1$ cm/s. In the first approximation, waves can be considered as standing in a fixed coordinate system because $|V_0/u_{0d2}| \ll 1$. A similar situation for micron size particles is described in [36]. Knowing the basic parameters of the dusty plasma, we turn to the calculation of the parameters of the nonlinear waves.

2.3. Hydrodynamic Wave Model

We assume that in the unperturbed state, the dust particles of the second fraction are affected only by the electric force F_{E2} and the neutral drag force F_{nd2} (due to the particle drift directed upward). Other forces are negligible (Table 2). The waves have almost no effect on the parameters of the first fraction, so we assume that $N_{d1} = n_{d1}/n_{0d1} = 1$. The dynamics of dust particles can be described by a system of one-dimensional hydrodynamic equations. In the frame of the second fraction—namely, in the frame moving upward with the speed u_{0d2} , the equations take the following form:

$$\frac{\partial v_{d2}}{\partial t} + v_{d2} \frac{\partial v_{d2}}{\partial z} = -\frac{eZ_2}{m_{d2}}(E + E') - \nu_{nd2}(v_{d2} - u_{0d2}) \quad (5)$$

$$\frac{\partial n_{d2}}{\partial t} + \frac{\partial n_{d2}v_{d2}}{\partial z} = 0 \quad (6)$$

where v_{d2} , n_{d2} , m_{d2} are the velocity, density, and mass of the second fraction particles, $E' = -\partial\phi/\partial z$ is the electrostatic field of the wave, ϕ is potential, and ν_{nd2} is the dust-neutral collisions frequency, which is easy to find from Equation (4); all other parameters are listed in Tables 1 and 2. Considering that $\sum F_0 = 0$, where F_0 is zero-order forces (i.e., $\nu_{nd2}u_{0d2} - eZ_2E/m_{d2} = 0$), Equation (5) can be rewritten as

$$\frac{\partial v_{d2}}{\partial t} + v_{d2} \frac{\partial v_{d2}}{\partial z} = -\frac{eZ_2}{m_{d2}}E' - \nu_{nd2}v_{d2}. \quad (7)$$

In the first approximation, considering $\nu_{nd2}v_{d2} = 0$, in the stationary case, according to [34], Equations (6) and (7) can be converted to the following form:

$$N_{d2}(\Phi) = \frac{n_{d2}}{n_{0d2}} = \frac{M}{\sqrt{M^2 + 2Z_2\Phi}}, \quad (8)$$

where $\Phi = e\varphi/C_{d2}^2m_{d2}$ is the normalized potential, $M = V/C_{d2}$ is the Mach number, and V is the steady-state wave velocity in the moving frame. The density of electrons and ions can be described by the Boltzmann distribution as follows:

$$N_e(\Phi) = \frac{n_e}{n_{0e}} = \exp\left(\frac{e\varphi}{T_e}\right) \equiv \exp\left(\frac{Z_2\Phi}{\delta_1 + \beta\delta_2}\right), \quad (9)$$

$$N_i(\Phi) = \frac{n_i}{n_{0i}} = \exp\left(-\frac{e\varphi}{T_i}\right) \equiv \exp\left(-\frac{Z_2\Phi\beta}{\delta_1 + \beta\delta_2}\right), \quad (10)$$

where $\beta = T_e/T_i$, $\delta_1 = n_{0e}/Z_2n_{0d2}$, $\delta_2 = n_{0i}/Z_2n_{0d2}$. Equations (8)–(10) are connected with the stationary Poisson equation.

$$\frac{d^2\Phi}{dS^2} = \frac{1}{Z_2}(\delta_1N_e - \delta_2N_i + \delta_3N_{d2}), \quad (11)$$

where $S = (z - Vt)/\lambda_{Di}$, $\delta_3 = n_{0d1}/Z_2n_{0d2}$. The quasi-neutrality condition yields $\Delta_1 - \Delta_2 + \Delta_3 + 1 = 0$.

Equation (11) can have solutions in the form of a soliton, nonlinear (cnoidal) wave, or linear wave, depending on the initial conditions. To describe large-amplitude soliton-

like dust-acoustic waves, we use the soliton solution of Equation (11). Such solutions of Equation (11) are well studied (see, for example, [1]). Figure 1 shows the numerically obtained soliton profiles at $M = 1.55$ and $M = 1.7$. Other parameters of the model are $\beta = 222$, $\Delta_1 = 0.135$, $\Delta_2 = 3.16$, $\Delta_3 = 2.03$ (Table 2). When integrating, the Runge–Kutta algorithm is used, the boundary conditions are as follows: $\Phi(-10) = -5 \times 10^{-4}$ and $\Phi'(-10) = 10^{-5}$ at $M = 1.7$; $\Phi(-10) = -8 \cdot 10^{-4}$ and $\Phi'(-10) = 10^{-5}$ at $M = 1.55$.

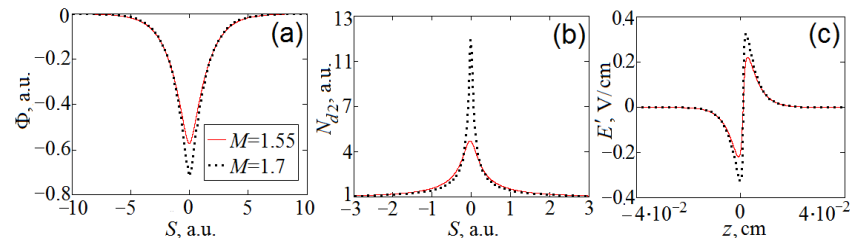


Figure 1. Soliton profiles with $M = 1.55$ and $M = 1.7$: (a) potential; (b) density of the second fraction particles; (c) electric field of the soliton.

From Figure 1, it can be seen that the wave width is $\Delta\varphi \approx 3\text{--}5 \lambda_{Di}$, and the width of the particle density profile is $\Delta N_{d2} \approx 1 \lambda_{Di}$. Our simple “cold” plasma model does not take into account the pressure of the dust fraction. However, in more realistic and complex models, the width of solitons can increase by several times (see, for example, the “warm” plasma model in [1]). Therefore, we assumed $\Delta N_{d2} = 3\lambda_{Di}$ in the above reasoning. The density of dust in the center of the soliton is increased up to 4–10 times. With such an increase in density, the soliton-like profiles can be easily observed in the optical range due to light scattering.

The electric field inside the soliton is perturbed by the value of $\Delta E' < 0.5 \text{ V/cm}$ (Figure 1c). Due to the fulfillment of the inequality $\Delta E' \ll E$, the nonlinear waves do not have a noticeable effect on the first fraction particles, which is confirmed experimentally. The wave velocity is $V = 7 \text{ cm/s}$, which corresponds in order of magnitude to u_{0d2} , but this is not enough for the observed slow wave motion downward in a fixed coordinate system. For a more accurate description of the experiment, additional research is needed. We return to this issue in the discussion.

3. Discussion

The reasons for the instability excitation can be ions (electrons) drift and ion drag force [37–42], dust charge perturbation [43–45], neutral drag force caused by the dust drift relative to a stationary neutral gas [46]. The third reason, in our opinion, dominates in the case under consideration. Indeed, first, the instability conditions obtained in [46] are satisfied, such as $n_{0e}/n_{0i} \ll 1$ and $E/N > E_{crit}/N$, where E_{crit} is the minimum value of the electric field sufficient to excite the instability. Secondly, the nonlinear waves are plane, occupying almost the entire radial cross section of the tube, far beyond the boundaries of the large particles cloud. The neutral drag force can be considered constant in the radial direction. The electric forces and the ion drag force should have a radial gradient, as evinced by the shape of the large particles cloud. If the forces of F_{E2} and F_{id2} caused the instability, the solitons would have a lenticular shape. The radial homogeneity of solitons can also be explained by the small charge of condensed particles ($Z_2 \sim 1$) since the discharge boundaries do not affect them significantly. A detailed analysis of the causes of instability is certainly of interest and will be carried out in the future.

In conclusion, we highlight the finding that continuous ion sputtering of the cone surface should lead to a loss of its mass Δm , which can be estimated by the formula $\Delta m = m_{d2} \cdot n_{0d2} \cdot \pi \cdot R^2 \cdot u_{0d2} \cdot \Delta t$. During the experiment $\Delta t \approx 1.2 \cdot 10^3 \text{ s}$, the mass loss can be neglected, as $\Delta m < 10^{-6} \text{ kg}$.

4. Experiment

The experiments were carried out in the Janis SVT-200 cryostat, which allows operation within the temperature range from 1.5 to 300 K [25]. A DC glow discharge was created in helium gas inside a vertical glass tube with an inner diameter of 2 cm. The distance between electrodes was equal to 60 cm. The experimental setup is shown schematically in Figure 2a. Polydisperse CeO₂ particles (0.1–200 μm) were used to form a dust cloud in the lowest stratum of the discharge.

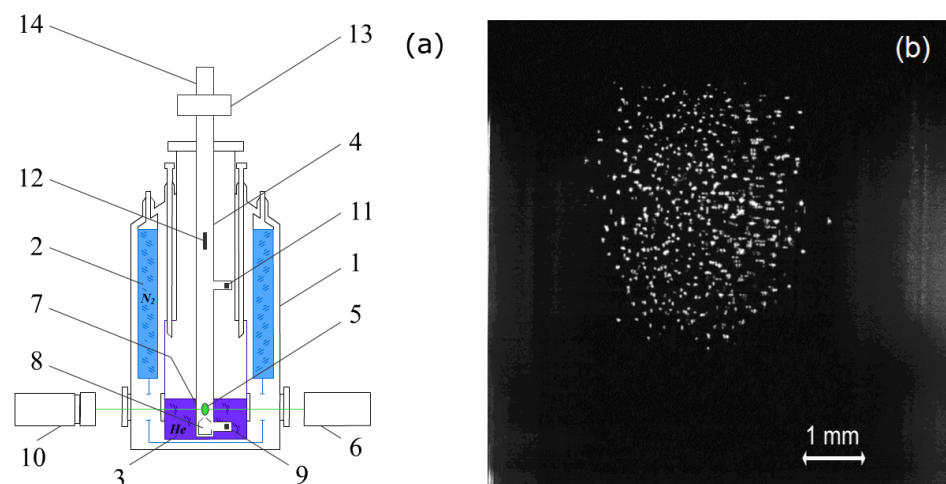


Figure 2. (a) Scheme of the experimental setup: 1—cryostat; 2—liquid nitrogen bath; 3—liquid helium bath; 4—gas discharge tube; 5—dusty plasma structure; 6—laser; 7—thermometer on the wall of the discharge tube; 8—dielectric cone; 9—cathode; 10—video camera; 11—anode; 12—dust particle injector; 13—cross-shaped connector; 14—pressure sensor; (b) initial dust cloud.

The pressure was measured using a Granville-Phillips 275 convectron, while the temperature was determined by a LakeShore 335 temperature controller connected to the TPK-1.5/60-22 semiconductor sensor calibrated within the working range of 1.5–60 K and attached to the discharge tube wall at the level of the lowest stratum. The waves were recorded using a high-speed digital camera (up to 1000 fps), a “laser knife” (with the cross section of 0.22×6 mm, 85 mW at 532 nm) was used for illumination of the dust cloud.

The operating temperatures were achieved by reducing the discharge current to 35 ± 15 μA at a voltage of 3.2 kV and a pressure of 5 Pa. In such a low-power mode, the temperature gradient between the anode and cathode did not exceed 2–3 K. As shown in Figure 2b, the initial shape of the dust cloud is close to spherical, the mean interparticle distance was ≈ 170 μm. At the same time, the particles formed the structure of the liquid type, containing randomly moving fast and slow particles. Fast particles formed intense vortex flows on the periphery of the cloud.

Approximately 20 min after the discharge had been generated, we detected scattering of laser radiation on moving local inhomogeneities as shown in Figure 3. At about the same time, the average distance between micron size particles decreased to ≈ 120 μm. It is clear from Figure 3, that there are no visible separate particles in the inhomogeneities. These facts indicate the appearance of a new submicron dust fraction, which was formed in the plasma during the experiment. The geometry of moving inhomogeneities indicates the excitation of dust-acoustic instability involving submicron particles. In what follows, subscripts 1 and 2 refer to injected (micron) and condensed (submicron) dust particles, respectively. As shown in [24], the appearance of fraction 2 was due to ionic sputtering of the dielectric cone material (8 on Figure 2a). The cone was used to focus the flow of electrons on the axis of the discharge tube. A flow of ions was also focused in the region of the cone and sputtered its surface. This hypothesis was confirmed during an additional experiment carried out at room temperature, which revealed an intense glow near the cone outlet. It is well known that polymer surfaces are easily sputtered in strata of the DC

glow discharge [47,48]. Therefore, we can expect rather an efficient sputtering of the cone material because it contains acrylic polymer [24]. The condensed fraction properties were studied in detail in a few studies [23,24].

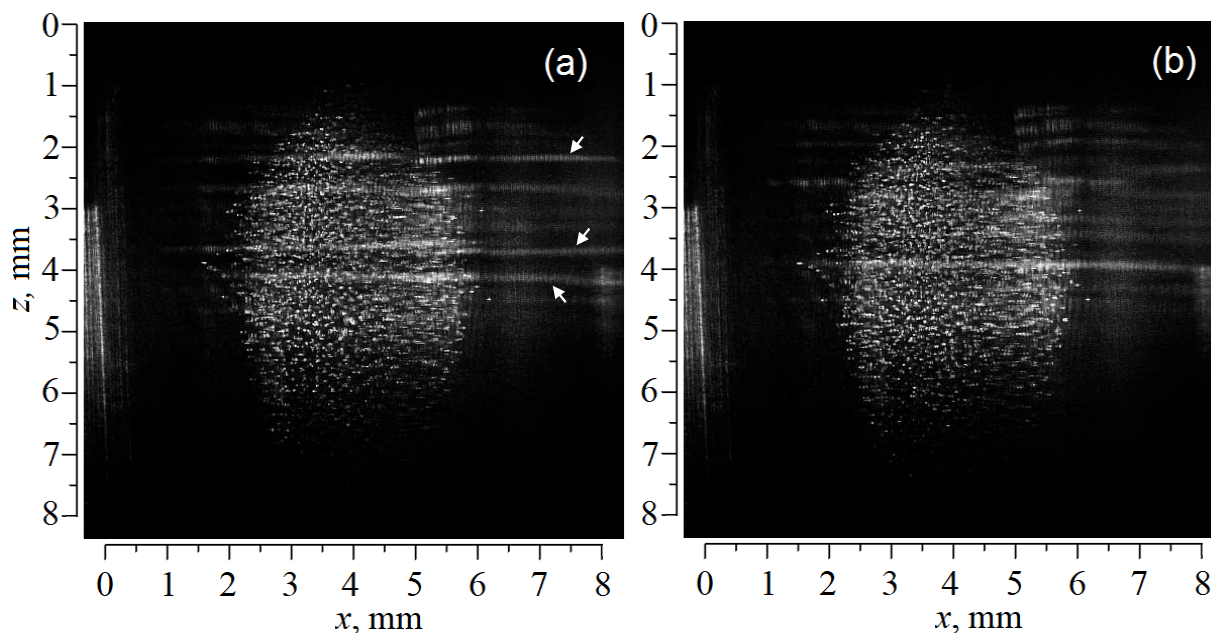


Figure 3. Dust cloud in the DC discharge stratum containing a mixture of the CeO_2 particles and condensed submicron particles formed 20 min after the start of the experiment; (a) $t = 0$; (b) $t = 30$ ms. The positions of large-amplitude wave crest are indicated by arrows.

The shape of the condensed particles is close to spherical, and the diameter does not exceed 75 nm with a large dispersion. The appearance of the condensed fraction led to some changes in the parameters of the initial dust cloud. For example, as mentioned above, the density of large particles increased (probably due to a decrease in the charge of large particles with the appearance of an additional submicron dust fraction and, therefore, due to competition for electrons and ions). A detailed study of the effect of fraction 2 on the evolution of the cloud is beyond the scope of this work. Notably, some parameters of the discharge slowly changed during the experiment. For example, the temperature of liquid helium varied in the range from 1.6 to 2.17 K. The main parameters of the discharge are listed in Table 1.

Considering the waves in fraction 2, as can be seen from Figure 3, fraction 2 fills a wider part of the tube than fraction 1. The waves were investigated in the same axial region where the particles of fraction 1 levitated. The observed wave process was rather complicated. However, some of its features can be considered. We use the one-dimensional approximation since the waves can be considered planes. Once the axis OZ is directed vertically downward (from the anode to the cathode), it can be inferred that the wave perturbation of the submicron particle (fraction 2) density cannot be described by a harmonic function ($\Delta n_{d2} \neq \exp(i\omega t + ikz)$). Indeed, the width of the compression regions, Δ_+ , is noticeably smaller than the width of the rarefaction regions, Δ_- ; therefore, the waves are nonlinear. In addition, $\Delta_+ \approx 100 \mu\text{m}$ for all cases, while Δ_- depended on z and t . Such behavior is characteristic of strongly nonlinear waves. The amplitudes of the individual wave crests were especially large (bright bands on Figure 3). These crests had soliton-like dust density profiles. The speed of the nonlinear waves was different in different parts of the dust structure but did not exceed 1 cm/s ($V \leq 1$ cm/s). According to our estimates (see below), the dust-acoustic velocity for the submicron dust fraction should significantly exceed the observed wave velocity ($C_{d2} \gg V$). Such a low velocity of nonlinear dust-acoustic waves can be explained either within the framework of the model [49] (where the self-consistent charge of particles was taken into account), within the framework of

research [50] (where dust compression waves in electrorheological dusty plasma were studied), or by the presence of submicron particle drift (second fraction particles). Under the considered experimental conditions, the drift hypothesis appears to be the most reasonable. It is important that the drift velocity of the second fraction particles should be approximately equal to the phase velocity of the waves. The effect of the observed waves on the particles of the first fraction was insignificant. Consequently, the electric field of the discharge significantly exceeded the electric field of the waves. We use standard models of a glow discharge dusty plasma for the theoretical interpretation of the experiment. The hydrodynamic model is used to calculate the parameters of the waves.

5. Conclusions

The nonlinear dust-acoustic instability excited in the condensed submicron fraction of dust in the four-component dusty plasma of the DC glow discharge at the gas temperature of ~ 2 K was studied in detail. The plasma contained injected CeO_2 particles of micron size and condensed nanoparticles, as well as electron and ion background. The nanoscale fraction was aggregated from products of ion sputtering of the polymer cone, which performed the function of focusing the electron stream. To analyze the observed waves, a simple hydrodynamic model was used, which made it possible to estimate important discharge parameters: λ_{Di} , T_i , particle drift velocities, etc. Independently of other authors [16–22], it was shown that the ions in the discharge are overheated in the presence of a significant electric field. The screening length was determined by the ions ($\lambda_D \approx \lambda_{Di}$). The obtained estimates for λ_{Di} are in good agreement with the results of [9] and are several times higher than the estimates of [4,6]. This discrepancy is due to the fact that $T_i = T_a$ was assumed in [4,6], while our analysis resulted in $T_i \gg T_a$. Estimates of other discharge parameters—namely, E/N , l_i , are consistent with [4].

Analysis of the acting forces showed that the second (invisible) fraction of dust drifts upward at the speed exceeding the dust-acoustic speed several times. The calculated electric field of strongly nonlinear waves proved to be an order of magnitude smaller than the field of discharge, which explains the absence of a relationship between waves and micron particles of the first fraction. The reasons for the excitation of the instability were briefly considered. The most likely cause is the neutral drag force, arising in the presence of significant drift of the second fraction particles. The linear stage of such instability was theoretically considered in [46].

In accordance with the assumptions made, the wave velocity V must be either equal to or slightly higher than the drift velocity u_{0d2} (i.e., $V \geq u_{0d2}$). In our estimates, the soliton velocity and the drift velocity coincide only in order of magnitude; what is more, $V < u_{0d2}$. One can achieve the fulfillment of the condition $V = u_{0d2}$ in two ways. First, by increasing the velocity of the nonlinear waves to $M \sim 4$ –5. Secondly, by reducing the drift velocity u_{0d2} . Future research will help clarify the values of V and u_{0d2} .

Author Contributions: Conceptualization, O.F.P., M.M.V., F.M.T. and R.E.B.; methodology, F.M.T., R.E.B., M.M.V. and O.F.P.; formal analysis, F.M.T. and R.E.B.; data curation R.E.B., O.F.P., M.M.V. and F.M.T.; writing—original draft preparation, O.F.P. and R.E.B.; writing—review and editing, F.M.T., R.E.B., O.F.P. and M.M.V. All authors have read and agreed to the published version of the manuscript.

Funding: The study was supported by the Russian Science Foundation (Project No. 19-12-00354).

Institutional Review Board Statement: Not applicable.

Informed Consent Statement: Not applicable.

Data Availability Statement: The data presented in this study are available on request from the authors.

Conflicts of Interest: The authors declare no conflict of interest.

Sample Availability: Samples of polydisperse powder of CeO_2 are available from many providers of chemical compounds.

References

1. Shukla, P.K.; Mamun, A.A. *Introduction to Dusty Plasma Physics*; IoP Publishing Ltd.: Bristol, UK, 2002.
2. Mikikian, M.; Boufendi, L.; Bouchoule, A.; Thomas, H.M.; Morfill, G.E.; Nefedov, A.P.; Fortov, V.E.; The PKE–Nefedov Team. Formation and behaviour of dust particle clouds in a radio-frequency discharge: Results in the laboratory and under microgravity conditions. *New J. Phys.* **2003**, *5*, 19. [[CrossRef](#)]
3. Fortov, V.E.; Vasilyak, L.M.; Vetchinin, S.P.; Zimnukhov, V.S.; Nefedov, A.P.; Polyakov, D.N. Plasma-dust structures at cryogenic temperatures. *Dokl. Phys.* **2002**, *47*, 21. [[CrossRef](#)]
4. Antipov, S.N.; Asinovskii, E.I.; Fortov, V.E.; Kirillin, A.V.; Markovets, V.V.; Petrov, O.F.; Platonov, V.I. Dust structures in cryogenic gas discharges. *Phys. Plasmas* **2007**, *14*, 090701. [[CrossRef](#)]
5. Ishihara, O. Complex Plasma Research under Extreme Conditions. *AIP Conf. Proc.* **2008**, *1041*, 139.
6. Ishihara, O. Low-dimensional structures in a complex cryogenic plasma. *Plasma Phys. Control. Fusion* **2012**, *5*, 124020. [[CrossRef](#)]
7. Shindo, M.; Samarian, A.; Ishihara, O. Dynamics of Charged Dust near Liquid Helium Surface. In Proceedings of the 12th Asia Pacific Physics Conference JPS, Makuhari, Japan, 14–19 July 2013; Volume 1, p. 015049.
8. Polyakov, D.N.; Vasilyak, L.M.; Shumova, V.V. Synergetics of Dusty Plasma and Technological Aspects of the Application of Cryogenic Dusty Plasma. *Surf. Eng. Appl. Electrochem.* **2015**, *51*, 143. [[CrossRef](#)]
9. Samoilov, I.S.; Baev, V.P.; Timofeev, A.V.; Amirov, R.K.; Kirillin, A.V.; Nikolaev, V.S.; Bedran, Z.V. Dusty plasma in a glow discharge in helium in temperature range of 5–300. *J. Exp. Theor. Phys.* **2017**, *124*, 496. [[CrossRef](#)]
10. Sundar, S.; Moldabekov, Z.A. Ultracold ions wake in dusty plasmas. *New J. Phys.* **2020**, *22*, 033028. [[CrossRef](#)]
11. Maiorov, S.A.; Tkachev, A.N.; Yakovlenko, S.I. Metastable state of supercooled plasma. *Phys. Scr.* **1995**, *51*, 498. [[CrossRef](#)]
12. Asinovskii, E.I.; Kirillin, A.V.; Markovets, V.V.; Fortov, V.E. Change-over of the conductivity mechanism in a nonperfect helium plasma on cooling to ~5 K. *Dokl. Phys.* **2001**, *46*, 321. [[CrossRef](#)]
13. Killian, T.C.; Pattard, T.; Pohl, T.; Rost, J.M. Ultracold neutral plasmas. *Phys. Rep.* **2007**, *449*, 77. [[CrossRef](#)]
14. Hutchinson, H.; Haakonsen, C.B. Collisional effects on nonlinear ion drag force for small grains. *Phys. Plasmas* **2013**, *20*, 083701. [[CrossRef](#)]
15. Semenov, I.L.; Khrapak, S.A.; Thomas, H.M. Approximate expression for the electric potential around an absorbing particle in isotropic collisionless plasma. *Phys. Plasmas* **2015**, *22*, 053704. [[CrossRef](#)]
16. Ellis, H.W.; Thackston, M.G.; McDaniel, E.W.; Mason, E.A. Transport properties of gaseous ions over a wide energy range. Part III. *Atomic Data Nucl. Data Tables* **1984**, *31*, 113. [[CrossRef](#)]
17. Saito, N.; Kojima, T.M.; Kobayashi, N.; Kaneko, Y. Mobilities of He⁺, Ne⁺, Ar⁺, and Kr⁺ in He gas at 4.35 K. *J. Chem. Phys.* **1994**, *100*, 5726. [[CrossRef](#)]
18. Viehland, L.A.; Mason, E.A. Transport properties of gaseous ions over a wide energy range. PartIV. *Atomic Data Nucl. Data Tables* **1995**, *60*, 137. [[CrossRef](#)]
19. Maiorov, S.A. Ion drift in a gas in an external electric field. *Plasma Phys. Rep.* **2009**, *35*, 802. [[CrossRef](#)]
20. Khrapak, A.G.; Golyatina, R.I.; Maiorov, S.A.; Khrapak, S.A. Approximation of the Mobility of Atomic Ions of Noble Gases in Their Parent Gas. *High Temp.* **2020**, *58*, 545. [[CrossRef](#)]
21. Ramazanov, T.S.; Daniyarov, T.T.; Maiorov, S.A.; Kodanova, S.K.; Dosbolayev, M.K.; Zhankarashev, E.B. Ion heating in dusty plasma of noble gas mixtures. *Contrib. Plasma Phys.* **2011**, *51*, 505. [[CrossRef](#)]
22. Antipov, S.N.; Asinovskii, E.I.; Kirillin, A.V.; Maiorov, S.A.; Markovets, V.V.; Petrov, O.F.; Fortov, V.E. Charge and structures of dust particles in a gas discharge at cryogenic temperatures. *J. Exp. Theor. Phys.* **2008**, *106*, 830. [[CrossRef](#)]
23. Boltnev, R.E.; Vasiliev, M.M.; Kononov, E.A.; Petrov, O.F. Self-organization phenomena in a cryogenic gas discharge plasma: Formation of a nanoparticle cloud and dust-acoustic waves. *J. Exp. Theor. Phys.* **2018**, *126*, 561. [[CrossRef](#)]
24. Boltnev, R.E.; Vasiliev, M.M.; Kononov, E.A.; Petrov, O.F. Formation of solid helical filaments at temperatures of superfluid helium as self-organization phenomena in ultracold dusty plasma. *Sci. Rep.* **2019**, *9*, 3261. [[CrossRef](#)]
25. Boltnev, R.E.; Vasiliev, M.M.; Petrov, O.F. An experimental setup for investigation of cryogenic helium plasma and dusty plasma structures within a wide temperature range. *Instrum. Exp. Tech.* **2018**, *61*, 626. [[CrossRef](#)]
26. Trukhachev, F.M.; Petrov, O.F.; Vasiliev, M.M.; Tomov, A.V. Relationship between the dust-acoustic soliton parameters and the Debye radius. *J. Phys. Conf. Ser.* **2020**, *1556*, 012073. [[CrossRef](#)]
27. Liu, J.; Ma, J.X. Dust-acoustic soliton in a streaming plasma. *Chin. Phys. Lett.* **1997**, *14*, 432.
28. Kubota, J.; Kojima, C.; Sekine, W.; Ishihara, O. Coulomb cluster in a plasma under cryogenic environment. *J. Plasma Fusion Res. Ser.* **2009**, *8*, 286.
29. Uotani, N.; Kubota, J.; Sekine, W.; Chikasue, M.; Shindo, M.; Ishihara, O. Dust Charging in Collisional Plasma in Cryogenic Environment. *J. Plasma Fusion Res. Ser.* **2010**, *9*, 404.
30. Raizer, Y.P. *Gas Discharge Physics*; Springer: Berlin/Heidelberg, Germany, 1991.
31. Hornbeck, J. The drift velocities of molecular and atomic ions in helium, neon, and argon. *Phys. Rev.* **1951**, *84*, 615. [[CrossRef](#)]
32. Patterson, P.L. Temperature dependence of helium-ion mobilities. *Phys. Rev. A* **1970**, *2*, 1154. [[CrossRef](#)]
33. Khrapak, A.; Ivlev, A.V.; Morfill, G.E.; Thomas, H.M. Ion drag force in complex plasmas. *Phys. Rev. E* **2002**, *66*, 046414. [[CrossRef](#)]
34. Petrov, O.F.; Trukhachev, F.M.; Vasiliev, M.M.; Gerasimenko, N.V. Large-scale transport of charged macroparticles induced by dust-acoustic solitons. *J. Exp. Theor. Phys.* **2018**, *126*, 842. [[CrossRef](#)]
35. Kotsarenko, N.Y.; Koshevaya, S.V.; Kotsarenko, A.N. Dusty plasma in space. *GeofisicalInternacional* **1998**, *37*, 71. [[CrossRef](#)]

36. Fortov, V.E.; Hoefner, H.; Morfill, G.; Petrov, O.F.; Simonchik, L.V.; Thoma, M.; Truhachev, F.M.; Usachev, A.D.; Zobnin, A.V. Solitary model of charged particle transport in dusty plasma. In Proceedings of the 34th EPS Conference on Plasma Physics, Warsaw, Poland, 2–6 July 2007; Volume 315, p. 66.
37. Rosenberg, M. Ion- and dust-acoustic instabilities in dusty plasmas. *Planet. Space Sci.* **1993**, *41*, 229. [[CrossRef](#)]
38. Rosenberg, M. Ion-dust streaming instability in processing plasmas. *J. Vac. Sci. Technol. A* **1996**, *14*, 631. [[CrossRef](#)]
39. D'Angelo, N. Dusty plasma ionization instability with ion drag. *Phys. Plasmas* **1998**, *5*, 3155. [[CrossRef](#)]
40. Ivlev, A.V.; Samsonov, D.; Goree, J.; Morfill, G.; Fortov, V.E. Acoustic modes in a collisional dusty plasma. *Phys. Plasmas* **1999**, *6*, 741. [[CrossRef](#)]
41. Molotkov, V.I.; Nefedov, A.P.; Torchinsky, V.M.; Fortov, V.E.; Khrapak, A.G. Dust acoustic waves in a DC glow-discharge plasma. *J. Exp. Theor. Phys.* **1999**, *89*, 477. [[CrossRef](#)]
42. Khrapak, S.; Yaroshenko, V. Ion drift instability in a strongly coupled collisional complex plasma. *Plasma Phys. Control. Fusion* **2020**, *62*, 105006. [[CrossRef](#)]
43. Fortov, V.E.; Khrapak, A.G.; Khrapak, S.A.; Molotkov, V.I.; Nefedov, A.P.; Petrov, O.F.; Torchinsky, V.M. Mechanism of dust-acoustic instability in a direct current glow discharge plasma. *Phys. Plasmas* **2000**, *7*, 1374. [[CrossRef](#)]
44. Islam, M.K.; Nakashima, Y.; Yatsu, K. On low-frequency dust-modes in a collisional and streaming dusty plasma with dust charge fluctuation. *Phys. Plasmas* **2003**, *10*, 591. [[CrossRef](#)]
45. Mondal, K.K. Propagation of dust-acoustic waves in weakly ionized plasmas with dust-charge fluctuation. *Pramana-J. Phys.* **2004**, *63*, 1021. [[CrossRef](#)]
46. D'Angelo, N.; Merlino, R.L. Current-driven dust-acoustic instability in a collisional plasma. *Planet. Space Sci.* **1996**, *44*, 1593. [[CrossRef](#)]
47. Polyakov, D.N.; Shumova, V.V.; Vasilyak, L.M. Self-organization of Coulomb balls in glow DC discharge in neon at cryogenic temperature. *Plasma Sources Sci. Technol.* **2019**, *28*, 065017. [[CrossRef](#)]
48. Karasev, V.Y.; Dzljeva, E.S.; Pavlov, S.I.; Matvievskaia, O.V.; Polishchuk, V.A.; Ermolenko, M.A.; Eikhval'd, A.I.; Gorbenko, A.P. Surface modification of melamine formaldehyde resin particles in a stratified glow discharge in neon. *Contrib. Plasma Phys.* **2019**, *59*, e201800145. [[CrossRef](#)]
49. Trukhachev, F.M.; Petrov, O.F.; Vasiliev, M.M.; Sevryugov, E.Y. A new approach to analysis of dust-acoustic solitons with a self-consistent charge of dust particles. *J. Phys. A Math. Theor.* **2019**, *52*, 345501. [[CrossRef](#)]
50. Schwabe, M.; Khrapak, S.A.; Zhdanov, S.K.; Pustynnik, M.Y.; R ath, C.; Fink, M.; Kretschmer, M.; Lipaev, A.M.; Molotkov, V.I.; Schmitz, A.S.; et al. Slowing of acoustic waves in electrorheological and string-fluid complex plasmas. *New J. Phys.* **2020**, *22*, 083079. [[CrossRef](#)]